Energy 50 (2013) 493–500

Contents lists available at SciVerse ScienceDirect

Energy

journal homepage: www.elsevier.com/locate/energy

Heat transfer to the riser-wall of a circulating fluidised bed (CFB)

A. Brems [a], G. Cáceres [b], R. Dewil [a], J. Baeyens [c], F. Pitié [d,e,*]

[a] Department of Chemical Engineering, Chemical and Biochemical Process Technology and Control Section, Katholieke Universiteit Leuven, Heverlee, Belgium
[b] Facultad de Ingeniería y Ciencias, Universidad Adolfo Ibáñez, Peñalolén, Santiago, Chile
[c] Beijing University of Chemical Technology, School of Life Science and Technology, Beijing, China
[d] University of Warwick, School of Engineering, Coventry, UK
[e] Whittaker Engineering Ltd., Upper Hindwells, Stonehaven AB39 3UT, UK

ARTICLE INFO

Article history:
Received 8 August 2012
Received in revised form
27 September 2012
Accepted 10 October 2012
Available online 16 November 2012

Keywords:
Heat transfer
Wall-to-suspension
Riser
Correlations
Prediction
Coefficient of heat transfer

ABSTRACT

The circulating fluidized bed is of increasing importance for gas–solid and gas–catalytic reactions, for drying, and recently its use in solar energy capture and storage has been advocated. In all applications, the supply or withdrawal of heat is a major issue, and the heat transfer coefficient from the gas–solid suspension to the heat transfer surface needs to be determined as design parameter. The present paper investigates the heat transfer coefficient for different operating gas velocity and solids circulation flux, whilst covering the different hydrodynamic solid flow regimes of dilute, core–annulus or dense mode. Measured values of the wall-to-bed heat transfer coefficients are compared with empirical predictions of both Molodstof and Muzyka, and Golriz and Grace. The application of a packet renewal mechanism at the wall is also investigated, and introducing the predicted solid contact time at the wall provides a very fair estimate of the heat transfer coefficient.

1. Introduction

1.1. The CFB and heat transfer

The circulating fluidized bed (CFB) regime is of increasing importance for gas–solid reactions (e.g. combustion, calcination, SO_2 removal from combustion gases), for gas–catalytic reactions (e.g. maleic anhydride from butane, acrylonitrile, aniline), and for physical gas–solid processes such as drying or VOC adsorption. A recent development is the use of a circulating fluidized bed in solar energy capture and storage systems, to replace thermal fluids or molten salts as transfer and storage medium [1]. Reviews of the different gas–solid and gas–catalytic applications, including environmental and energy topics, are given in e.g. Mahmoudi et al. [2] and Chan et al. [3]. Fernandes et al. [4] illustrate applications in solar energy capture systems. Layouts of different applications are illustrated in Fig. 1

A CFB shares many of its advantages with traditional bubbling beds, including temperature uniformity and excellent heat transfer, while allowing higher gas throughput and having a greater ability to handle agglomerating particles. The circulation of particles requires solids' collection and return equipment: the overall CFB setup hence consists of a riser, a cyclone, a downcomer and a return valve (often executed as non-mechanical valve), as illustrated in Fig. 1.

Most reactions carried out in the CFB are endothermic or exothermic and hence require an exchange of heat between the gas–solid suspension and heat transfer surfaces, located either at the wall of the riser, inside the riser, externally in a low-velocity fluidized bed in the return loop of the solids, or as a traditional downstream heat exchanger on the exhaust gas (superheater or economizer tube-bundle). Mostly membrane water-wall surfaces are used in combustion or other exothermic applications. For other systems, it might be impossible to provide sufficient heat transfer surface at the wall of the riser (unless extremely tall). It is then necessary to embed surfaces in the riser itself, as is mostly the case for highly exothermic gas–catalytic reactions. In solar energy capture systems, solar heat will be directed onto the outside riser wall, and subsequently transferred to the circulating solids.

Given the wear caused by particles moving rapidly upwards and downwards, CFB reactors seldom employ internal surfaces. Hence, the design problem of greatest interest is how to predict the heat transfer coefficient at the wall of a CFB. In almost all cases of practical importance, the membrane surface wall is disposed in such a manner that the tubes are orientated vertically.

* Corresponding author. University of Warwick, School of Engineering, Coventry, UK.
E-mail addresses: fpitie@whittakereng.com, f.pitie@warwick.ac.uk (F. Pitié).

0360-5442/$ – see front matter
http://dx.doi.org/10.1016/j.energy.2012.10.037

Nomenclature

a, b	dimensionless parameters of Equation (4)
A_{ex}	surface area of the heat exchanger, m
C	solid to gas heat capacity, C_p/C_g
C_p, C_g	specific heat capacity of solid and gas respectively, J kg^{-1} K^{-1}
CAF	core–annulus flow
BFB, CFB	bubbling and circulating fluidized bed, respectively
ID, OD	inner and outer diameter respectively, m
D	riser equivalent diameter, m
d_p	average particle diameter, μm
DRF, DRU	dilute riser flow and dense riser up-flow respectively
f_d	time fraction of contact by the dense phase
G	solids circulation flux, kg m^{-2} s^{-1}
G_{sh}	particles horizontal exchange flux, kg m^{-2} s^{-1}
h_c	contact transfer resistance, W m^{-2} K^{-1}
h_d	heat transfer coefficient during dense phase contact, W m^{-2} K^{-1}
h_{ij}^{rad}	radiation heat transfer coefficient, W m^{-2} K^{-1}
h_g	heat transfer coefficient of gas, W m^{-2} K^{-1}
h_{gc}	gas convective transfer coefficient, W m^{-2} K^{-1}
h_l	heat transfer coefficient of lean gas phase contact, W m^{-2} K^{-1}
h_m	heat transfer coefficient of the suspension, W m^{-2} K^{-1}
h_r	heat transfer coefficient by radiation, W m^{-2} K^{-1}
h_{sr}	heat transfer coefficient by radiation from the suspension to the wall, W m^{-2} K^{-1}
h_{tot}	total effective heat transfer coefficient, W m^{-2} K^{-1}
$h(\overline{\theta})$	surface renewal heat transfer coefficient, W m^{-2} K^{-1}
k_g	thermal conductivity of gas, W m^{-1} K^{-1}
M	loading ratio
Nu	Nusselt number
Pr	Prandtl number
Re	Reynolds number
T_b, T_w	bulk and wall temperature, respectively, K
t_g, t_p	residence time of gas and particles in the riser, respectively, s
TFBB	turbulent fluidized bed at the bottom
U	superficial air velocity through the riser, m s^{-1}
U_{TR}	transport velocity of particles, m s^{-1}
$\overline{v}_p$	average velocity of particle, m s^{-1}
δ_g	gas gap thickness, μm
ΔT	temperature difference
ε	voidage of the riser
ε_B	voidage of the TFBB
ε_{sus}	cross sectional average suspension voidage
φ	slip factor
$\overline{\theta}$	average contact time of the particle packets at the wall, s
ρ_g, ρ_p	density of gas and solids respectively, kg m^{-3}
ρ_{sus}	suspension density, kg m^{-3}
ζ	$\zeta = \sqrt{1.82\log(Re) - 1.64}$

The design of the heat transfer surface requires the knowledge of the heat transfer coefficient between the flowing gas–solid suspension and the surface itself. The present paper investigates first results obtained towards the heat transfer coefficient as measured in a riser for Geldart A-type particles with average particle size of approximately 75 μm, representative of most industrial CFB applications. The objectives of the research objective were twofold: (i) to determine the wall-to-bed heat transfer coefficient for different operating conditions of gas flow and solids' circulation flux, thus covering the different operating modes of the riser flow (dilute, core–annulus, dense), and (ii) to compare experimental results with existing model approaches. The different operating modes have been classified by Mahmoudi et al. [2] in terms of the dominant flow parameters, being the superficial gas velocity, U, (corrected for the velocity of onset circulating mode, U_{TR}) and the solids circulation flux, G. The resulting diagram is represented in Fig. 2. Since solids flow modes will determine the heat transfer coefficient, a summary discussion of these flow modes will be given in Section 1.2.

The heat transfer to the wall of a CFB riser can be assumed to involve additive components due to conduction, convection and radiation. Many researchers have approached the phenomenon with a two-phase structure, somewhat similar to that described for bubbling fluidised beds (BFB) [5]. The two phases are however different from those in bubbling beds, since no bubbles are present, but with the flow at the wall in the core–annulus (CAF) operating

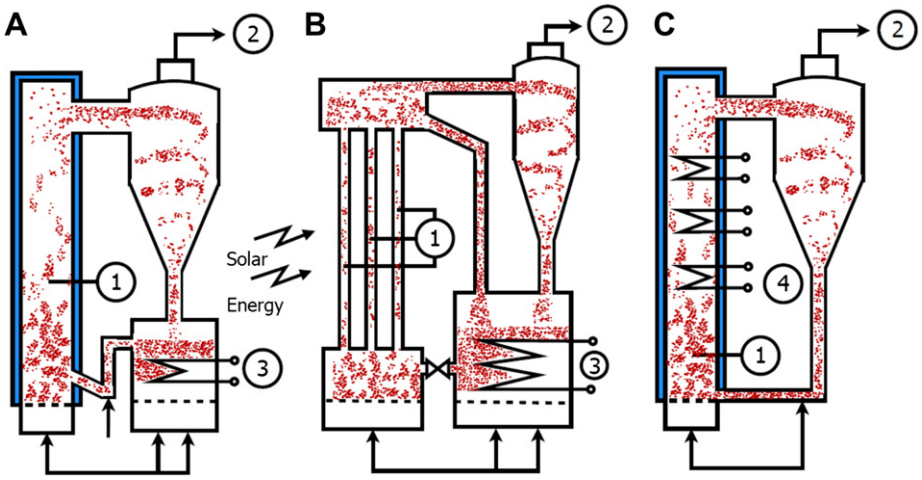

Fig. 1. Illustration of different CFB layouts, with heat transfer. (1) Riser, with wall-mounted heat exchanger in (A) and (C), (2) exhaust to further treatment or de-dusting, (3) heat exchange surface in secondary bubbling fluidised bed, (4) in-riser heat exchanger. (A) Application for gas–solid reaction, e.g. combustion. (B) Application in solar energy capture and storage. (C) Application for gas–catalytic reaction, with in-bed heat transfer.

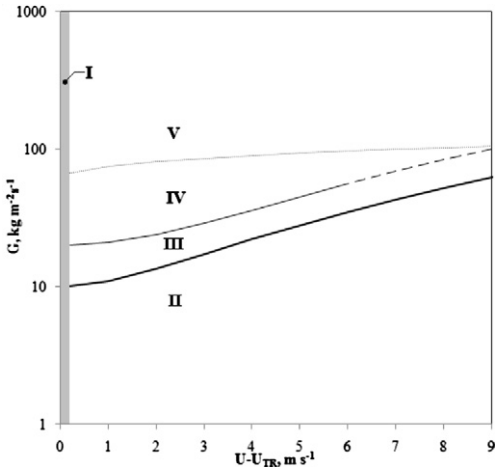

Fig. 2. Hydrodynamic operating modes of a CFB riser, expressed as G versus $U - U_{TR}$ depending on the different hydrodynamic flow modes [2]: Zone I: transition zone and/or inaccuracy in U_{TR} prediction, Zone II: dilute riser flow (DRF), Zone III: core–annulus flow (CAF) only, Zone IV: CAF with turbulent fluidized bed at the bottom (TFBB), Zone V: dense riser up-flow (DRU). ——— transition DRF – CAF: $G = 10 + (U - U_{TR})^{1.8}$, ——— transition CAF – CAF with TFBB: $G = 20 + (U - U_{TR})^2$, ····· transition CAF with TFBB – DRU: $G = 60 + 15\ (U - U_{TR})^{0.5}$, — — — range of operating conditions where CAF mode is no longer reported and only DRF and DRU prevail.

mode dominated by streamers or clusters travelling mostly downward, but interspersed with periods where there is upwards flow of the powder suspension. In dilute or dense riser flow, the solids flow is dominantly upwards. Complementing experiments in a bubbling bed, CFB experiments by Wu et al. [6] with small flush-mounted heat transfer surfaces have shown rapidly varying local instantaneous heat transfer coefficients, with the fluctuations corresponding to the arrival of streamers at the heat transfer surface. Hence, the processes governing heat transfer are indeed similar in BFB and CFB, with packets of particles contacting the wall, and exchanging heat according to the known film penetration model [7]. Several factors are however complicating the situation:

- The voidage distribution in bubbling beds is essentially binary, varying between a discrete dense phase voidage and nearly pure voids inside bubbles. The voidage distribution in a riser tends to be continuous and widely dispersed.
- The powder flow in the CFB riser can reverse directions, moving both upwards and downwards, especially in the CAF operating mode.

Boiler makers and other manufacturers of large CFB units estimate the heat transfer coefficient on confidential experience from previous units, with adjustments to account for such factors as changes in mean particle diameter, suspension density, and membrane surface geometry. Published empirical correlations, widely used in bubbling fluidized beds, are not common for circulating fluidized beds. Instead, two semi-empirical models have been proposed in the literature based on the periodic renewal of particle clusters at the heat transfer surface. As indicated in Equation (1), one treats the heat transfer as being additively composed of conduction/convection and radiation [8].

$$h_{tot} = f_d h_d + (1 - f_d) h_l + h_r \tag{1}$$

The experimental data available for predicting the heat transfer in CFBs are mostly from larger CFBs, with cross-sectional areas varying from 2.4 to 88 m^2, as summarized by Golriz and Grace [9]. While the limited number of data is a disadvantage, there is one significant advantage of larger scale equipment, being the fact that large risers are tall enough to guarantee that both the flow and the heat transfer are fully developed [9]. In small scale CFBs, relevant measurements should only be made in the fully developed riser flow, i.e. at a distance from the recycle entry and the exit geometry [10,11].

1.2. Operating hydrodynamic regimes in a CFB

The riser operating modes are vital to design a CFB for a required process. Different operating modes provide different solid residence times and mixing behaviour, which define both the efficiency/yield of the reactions and the heat transfer. Literature gives evidence of distinct operating modes as a result of observed differences both in slip factors, and in the range of particle velocities and their associated residence time distribution [2,10], resulting in the definition of 4 distinct solids hold-up regimes in the riser, as depicted in Fig. 2, with the different operating modes (dilute, dense, core–annulus, combined) being a function of U and G in the riser.

The various flow regimes have distinct characteristics towards solids flow, and hence towards heat transfer. For these different regimes, the particle velocity has been expressed by Equation (2), introducing the slip factor, φ, resulting in:

$$\overline{v}_p = \frac{U}{\varepsilon\phi} \tag{2}$$

In *Dilute Riser Flow (DRF)*, the solids are predominantly moving upwards with negligible downward flow. In DRF-regime, the slip factor, φ, has a previously reported value between 1 and 1.2 [3,12]. In *Core–annulus Flow (CAF)*, the solids motion is an upward core flow and unsteady downward (cluster or streamer) flow in the annulus. The solids velocity can be predicted by Equation (2), with φ values close to 2 [3,13,14]. The regime of the *Core–annulus Flow (CAF) with Turbulent Fluidised Bottom Bed (TFBB)* is characterized by an axial voidage profile of typical S-nature, due to the appearance of a Turbulent Fluidised Bottom Bed (TFBB). The residence time for CAF with TFBB is significantly longer than CAF itself and DRF due to the existence of the fully mixed TFBB. Chan et al. [11] demonstrated that the residence time for solids in TFBB alone can range from 10 to 20 s. The voidage of the TFBB ranges from 0.7 to 0.9 and can be predicted by the empirical Equation (3) [15]:

$$\varepsilon_B = \frac{U + 1}{U + 2} \tag{3}$$

The characteristics of the CAF region above the TFBB are similar to the above sole CAF flow, as described before. The *Dense Riser Upflow (DRU)* regime has almost similar characteristics to DRF, the main difference being that the φ values are fractionally higher, ranging between 1.2 and 1.6 with an average of 1.3 [3].

Average voidages in these various hydrodynamics regimes range from approximately 0.98 in dilute flow (DRF); 0.7–0.9 in a bottom fluidised bed (TFBB), 0.95–0.98 in core–annulus mode (CAF), to ~ 0.9 in dense riser up-flow (DRU) respectively [16–18].

Commercial risers of e.g. combusters and calciners, are reported in CAF operation in the range of $U - U_{TR} = 0.5$–5 m/s and G-values of 10 to about 80 kg/m^{2}s. CFB operations in DRU-mode are reported in mostly gas–catalytic operations for $U - U_{TR}$ values in excess of about 8 m/s and G-values between 150 and 1200 kg/m^{2}s. These reported combined (U,G) ranges are in good agreement with the proposed operation diagram of Fig. 2.

2. Previous work on heat transfer in a CFB riser

2.1. Molodtsof and Muzyka

Work undertaken on vertically flowing suspensions has been reviewed in great detail by Muzyka [19] and Grace [20]. As long as convective heat transfer between the suspension and the surface is considered, with the exclusion of radiant heat transfer, the major concern is to predict the variation of the heat transfer coefficient with solids loading and gas velocity in various riser geometries. Various empirical correlations and models (mostly for bed-to-wall heat transfer) have been proposed [6,21], but Grace [20] summarized the situation as follows: "no existing correlations give consistent agreement with the available data".

The theoretical approach proposed by Molodstof et al. [22] and by Molodstof and Muzyka [23] is based upon the rigorously derived general probabilistic equations for multiphase flow [24–26]. According to their treatment, the wall-to-suspension heat transfer coefficient can be expressed as a function of the loading ratio, M, and of the heat capacity ratio, C:

$$\frac{h_m}{h_g} = \frac{(1+MC)^2}{1+aMC+b(MC)^2} \tag{4}$$

The equation relates the heat transfer coefficient of the suspension, h_m, to that of the gas alone, h_g, flowing in the same pipe at the same gas flow rate. The loading ratio, M, expressed as kg solids/kg gas, together with the solids-to-gas heat capacity ratio, $C = C_p/C_g$, are the dominant parameters. The dimensionless parameters a and b in Equation (4) are compound factors involving dimensionless radial concentration, velocity, and temperature profiles. They are generally unknowns, as the profiles are unknown, and depend upon design parameters (pipe diameter, particle size distribution and physical properties), and upon the superficial gas velocity. With a and b fitted from experimental results for the specific gas–solid system under scrutiny, the trend of reported heat transfer results, obtained at a constant wall heat flux, was shown to be in good agreement with predictions of Equation (2) [19,27]. It was therefore considered interesting to assess the CFB-validity of Equation (4), as well as the effect of the flow structure on the heat transfer.

2.2. Golriz and Grace

Golriz and Grace [9] devised a model for large units based on the assumptions of fully developed conditions and radially uniform clusters at the wall, hence valid for CAF operation. At any instant, some portions of the surface are bare, while other portions of the surface are covered by clusters, each separated from the wall by a thin gas gap of thickness δ_g. Different heat transfer mechanisms are assumed for the bare and covered portions. For the bare sections, transfer is by gas convection (denoted by subscript 'gc') and by radiation from the suspension to the wall (subscript 'sr'). The rest of the wall is covered by clusters/streamers providing a parallel transfer path. The transfer rate is then assumed to be controlled by a particle horizontal exchange flux, G_{sh}. The combined expression of the heat transfer coefficient is given as a total heat transfer coefficient, h_{tot}, as follows:

$$h_{tot} = (h_{gc}+h_{sr})\,(1-f) + \frac{f}{\dfrac{1}{G_{sh}C_p + h_{be}^{rad}} + \dfrac{1}{(k_g/\delta_g)+h_{ew}^{rad}}} \tag{5}$$

For operation at temperatures below 600 °C, the radiation contribution is negligible [5].

The parameters of the equation are correlated by different equations.

The fractional coverage, f, accounts for the scale of the unit as follows:

$$f = 1-\exp\left[-25{,}000\left(1-\frac{2}{\exp(0.5D)+\exp(-0.5D)}\right)(1-\varepsilon_{sus})\right] \tag{6}$$

where D is the riser equivalent diameter (4× cross sectional area/perimeter) in metres. For large units, f approaches unity, meaning that the entire wall becomes covered by clusters. An alternative relationship giving somewhat lower values of f as D increases, has been suggested by Dutta and Basu [28]. The gas convective transfer coefficient, h_{gc}, was obtained from the well-known Dittus–Boelter correlation [29].

The gas gap thickness is estimated [30] from:

$$\delta_g = 0.0282\, d_p (1-\varepsilon_{sus})^{-0.59} \tag{7}$$

An expression for the lateral solids flux was obtained by fitting all heat transfer data for units of hydraulic diameter ≥ 1 m where the suspension densities, $\rho_{sus} = \rho_p(1-\varepsilon_{sus}) + \rho_g\varepsilon_{sus}$, were greater than or equal to 5 kg/m^3, leading to:

$$G_{sh} = 0.1093 + 0.0225\ln(\rho_{sus}) \tag{8}$$

Radiation between the suspension and the bare wall was estimated from a parallel surface expression, with equations provided in the original work [9]. The fundamental radiation approach of Gorliz and Grace can however be simplified. The effect of operating at higher temperature, i.e. generally >600 °C, is twofold and includes the effect of both the increasing thermal properties of mainly the gas phase, and the direct contribution of radiation heat transfer. The effect of the thermal properties of the fluidizing gas is reflected to a major extent in the temperature dependence of the increasing gas thermal conductivity as T increases, and increasing the heat transfer coefficient proportionally with $\sqrt{k_g}$ [5,7]. The additive effect of radiation itself is expressed in Equation (1), with an increasing contribution to heat transfer as T increases [31], however function of the size and nature of the fluidized solids. Adapted results of Baskakov [31] are illustrated in Fig. 3 for particle sizes as commonly used in CFB applications. This figure provides a rule of thumb estimate.

The radiation component can also be estimated by using the Stefan–Boltzman equation:

$$h_r = 5.673 \times 10^{-8}\ \varepsilon_r\left(T_w^4 - T_b^4\right)\Big/(T_w - T_b) \tag{9}$$

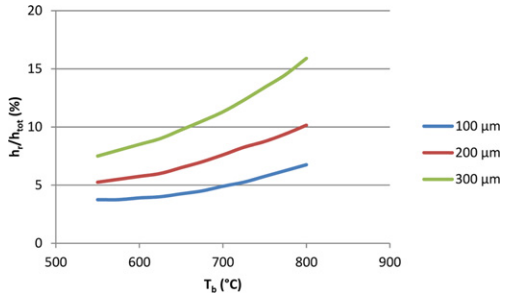

Fig. 3. Fractional component of total heat transfer coefficient attributable to radiation, wall temperature 850 °C, and for three mean particle sizes (adapted from Baskakov [31]).

with wall (T_w) and bed (T_b) temperatures in absolute values, and ε_r as reduced emissivity to account for the different emissive properties of the surface (ε_s) and bed (ε_b), according to:

$$\varepsilon_r = 1/[(1/\varepsilon_s + 1/\varepsilon_b) - 1] \quad (10)$$

ε_b assumes values of 0.59 for Al_2O_3 and ZrO_2, 0.8 for clay, 0.85 for sand and 0.95 for fused MgO.

Because of the effect of the hot surface on the immediately adjacent particles, the bed temperature there will be higher than the bulk temperature, and allowance should be made for this when using the bulk temperature in Equation (10). Baskakov [31] suggests to use an apparent emissivity (ε_{app}) instead of ε_r. The values of ε_{app} will be a function of the operating temperatures, as illustrated in Baskakov [31]. A reasonable value for alumina would be between 0.6 and 0.7, and somewhat lower for sand.

ε_r may be as low as 0.1 when using a shiny metal surface.

2.3. The surface renewal model

Since the heat transfer is determined by the transient heat transfer of the transfer wall to packets of particles in contact, a surface renewal model can possibly be applied, as developed by Baeyens and Geldart [5] for bubbling fluidized bed applications.

$$h\left(\overline{\theta}\right) = \frac{h_c}{1 + \dfrac{6h_c}{\rho_p C_p d_p}\overline{\theta}} \quad (11)$$

where $h(\overline{\theta})$ is the average heat transfer coefficient from the suspension to the wall, h_c is a contact transfer resistance, and $\overline{\theta}$ is the average contact time of the particle packets at the wall. The experimental results will also be used to check the applicability of such a packet renewal mechanism.

3. Experimental setup and procedure: wall-to-bed heat transfer

The riser and CFB are depicted in Fig. 4. The riser consists of a 50 mm ID pipe approximately 2.5 m high. Solids circulation was achieved via a 100 mm ID downcomer and 50 mm ID L-valve. Air is supplied through a distributor plate and leaves the system through a cyclone after the riser exit. Pressure taps are located along the height of the riser and connected to a data acquisition system. Flow rates and pressure drops were monitored. A concentric wall heater of 10 cm length was installed at 1.2 m above the re-entry joint of the L-valve, hence within the fully-developed riser flow mode. Heat supply was by hot water or thermal fluid (Santotherm 350). The downcomer was water-cooled through a 0.2 m long concentric cooler. The wall surface temperature was measured using a resistance thermocouple welded onto the wall. Additional Thermocoax thermocouples (0.1 mm OD) were installed at various locations in the riser and downcomer, as well as in the feeding and overflow lines of the fluid, as indicated in Fig. 4. The heat input was set at such a value, that the bed temperature ranged from 30 to 40 °C.

The experiments consisted of starting the gas flow to the riser, followed by the flow of the fluidizing gas to the solids feeder.

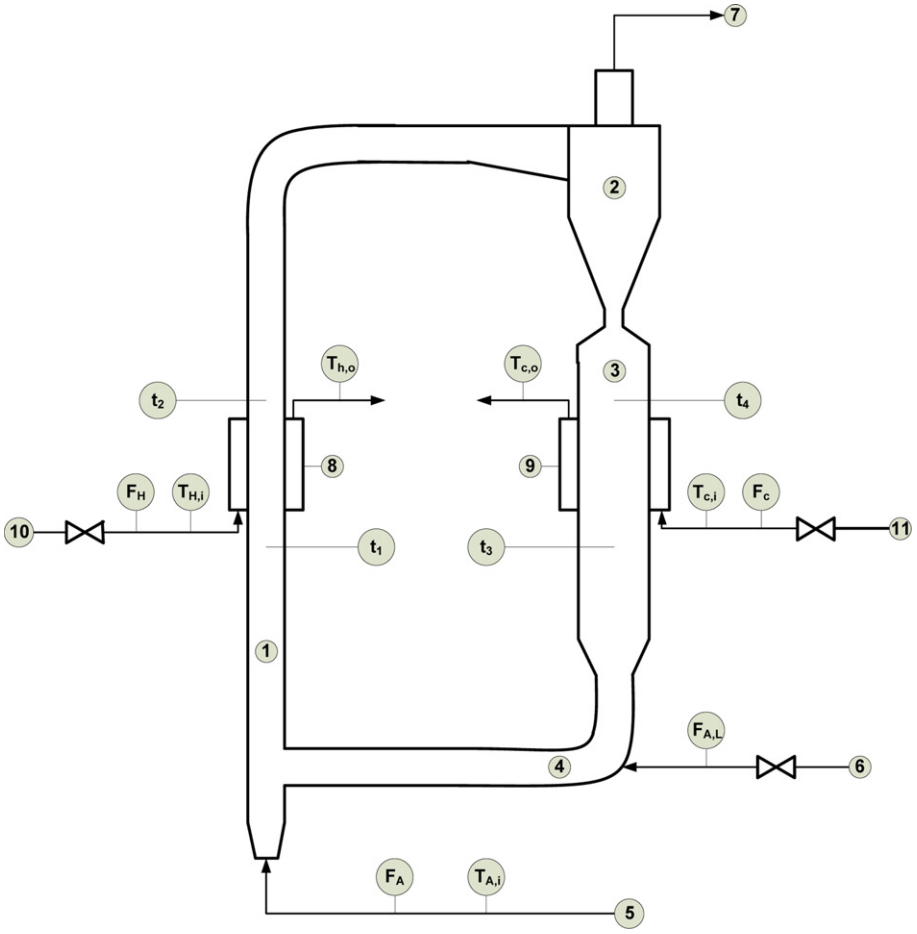

Fig. 4. Layout of the experimental set-up: (1) riser 50 mm I.D., (2) HE Stairmand cyclone, (3) downcomer 100 mm I.D., (4) L-valve 50 mm I.D., (5) air from speed-controlled blower, (6) compressed air, (7) vent to baghouse filter, (8) co-axial heating section, (9) co-axial cooling section, (10) supply of thermal fluid, (11) supply of cooling water; F_H, F_C, F_A, $F_{A,L}$: respectively flow metres of thermal fluid, cooling water, riser air, L-valve air; T: temperature probes for respective fluids; t: temperature probes inside riser and downcomer.

The flow rates of gas and solids were then set to the desired values, the heat input into the system was fixed, and the system was allowed to stabilize over a period of about 1 h, during which flow rate, temperatures, and pressures were monitored and recorded.

The axial pressure profile was recorded during each experiment in order to make sure that the suspension entering the heated section was in fully developed flow conditions.

From the known exposed surface area, A_{ex}, and measured temperature difference, ΔT, the heat transfer coefficient was calculated for the given heat input as:

$$h_m = \frac{Q}{A_{ex}\Delta T} \tag{12}$$

The measurements were performed for the gas flow alone and for the gas–solid suspension at various solid/gas ratios. The heat transfer coefficient to the gas–solid suspension, h_m, was also expressed as h_m/h_g ratio. The bed material used was rounded sand of the following characteristics: $d_p = 75$ μm, $\rho_p = 2260$ kg/m^3, and $C_p = 1.05$ kJ/kg K.

Various combined (U,G) values were tested in order to scan the different riser hydrodynamic regimes: these conditions are illustrated in Fig. 5, using the Mahmoudi et al. [2] regime diagram as a basis. Clearly, all operating modes were assessed by the experiments.

4. Results and discussion

4.1. Preliminary literature findings

In a previous research, Everaert et al. [32] studied the heat transfer coefficient to an in-bed heat transfer surface in a 0.1 m I.D. riser, expressed as h_m and related to the sole gas flow convection heat transfer coefficient h_g. Experiments were carried out in the DRF and CAF operating modes. It was demonstrated that (i) the heat transfer coefficient in the core is significantly higher than at the wall; (ii) the core region extends to approximately 85% of the riser radius (0.05 m), hence with an annulus thickness of approximately 7.5 mm; and (iii) increasing the gas flow rate at a given solid circulation rate significantly reduces the suspension heat transfer coefficient.

The Everaert et al. [32] paper moreover quantitatively determines the radial dependence of the heat transfer coefficient, as illustrated in Fig. 6.

It can be seen that the wall-to-bed heat transfer coefficient is about 20–40% lower that the in-bed surface heat transfer coefficient. Even in dilute flow, i.e. at the low G values of Fig. 6, the solids contribute significantly to the overall heat transfer coefficient, since the ratio h_m/h_g exceeds ~2.

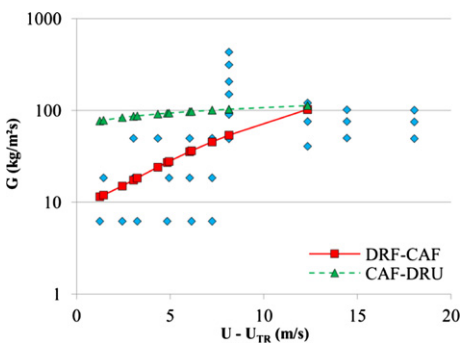

Fig. 5. Experimental (U,G) conditions in comparison with the riser flow modes.

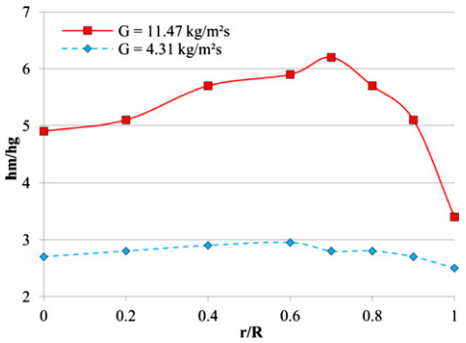

Fig. 6. Effect of the radial position of the heater in the riser on the heat transfer coefficient h_m (expressed as ratio) at $U_g = 7.8$ m/s.

4.2. Experimental results for the riser-wall to bed heat transfer coefficient, h_m

Experimental results are illustrated in Fig. 7 as h_m/h_g-ratio. h_m is a strong function of the (U,G) combination, especially at lower G values, thus also of the hydrodynamic operating mode of the riser. Experimental results will further be developed in terms of the approaches of Section 2.

At $G = 0$, h_m should assume the h_g heat transfer coefficient, only a function of U.

4.3. Transformation of experimental results into design equations

4.3.1. The gas convection coefficient

Essential in the use of the semi-experimental equations, is the prediction of the heat transfer coefficient when solids are absent, i.e. the heat transfer coefficient between the heat transfer surface and a pure gas flow in the riser, h_g. The equation used to predict h_g in the present treatment was presented by Gnielinski to cover gas flow in the transitional and turbulent flow regime [33].

$$Nu = \frac{h_g D}{k_g} = \frac{\left(\frac{\zeta}{8}\right)(Re - 1000)Pr}{1 + 12.7\sqrt{\frac{\zeta}{8}}\left(Pr^{2/3} - 1\right)}\left(1 + \left(\frac{D}{L}\right)^{2/3}\right) \tag{13}$$

with $\zeta = \sqrt{1.82\log(Re) - 1.64}$ and other symbols defined in the Nomenclature.

4.3.2. Molodtsof and Muzyka

All results were expressed as h_m/h_g values. Experimental results, at constant value of C and varying value of M, were used to determine coefficients a and b, whilst then comparing the trend of h_m/h_g

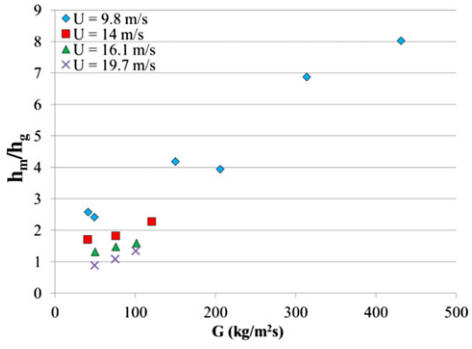

Fig. 7. Experimental results, expressed as h_m for different (U,G) combinations.

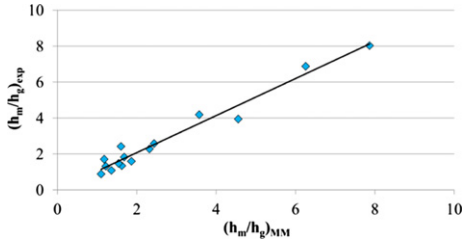

Fig. 8. Comparison of experimental and Molodstof–Muzyka (MM) predicted values of h_m/h_g.

as predicted by Equation (4). Results are given in Fig. 8, illustrating the fair agreement obtained, with coefficients a and b respectively 3.54 and 0.034, and with a regression coefficient $R^2 = 96.47\%$. Of course, the design application of the Molodtsof and Muzyka approach needs experimental determination of coefficients a and b.

4.3.3. Golriz and Grace

The empirical equations of Golriz and Grace [9] can be transformed into the following equation, when radiation is neglected.

$$\frac{h_m}{h_g} = (1-f) + \frac{f}{\left(\frac{1}{G_{sh}C_p} + \frac{1}{k_g/\delta_g}\right)} \tag{14}$$

The suspension voidage and density was calculated according to Chan et al. [3], with t_p and t_g the residence times of the particles and the gas in the riser respectively. The values of t_g were calculated by the method presented in Mahmoudi et al. [16].

$$\varepsilon_{sus} = \frac{Ut_g}{Ut_g + Gt_p/\rho_p} \tag{15}$$

$$\rho_{sus} = \varepsilon_{sus}\rho_g + (1-\varepsilon_{sus})\rho_p \tag{16}$$

Since Golriz and Grace only deal with CAF applications ($G < \sim 100$ kg/m^{2}s) in large scale risers, experimental results of the CAF regime were compared with predicted values, as illustrated in Fig. 9A.

The deviation is between ~250 and 350%. Reasons are inherently linked to the difference in equipment scale, and to the required calculation of the underlying parameters, again on the basis of empirical approaches. A sensitivity analysis of the Gorliz–Grace approach pointed out that the predicted heat transfer coefficient is highly sensitive to the empirical parameter G_{sh}, as predicted by Equation (8). A very fair agreement of the present experimental and Gorliz–Grace predicted h_m/h_g ratios was

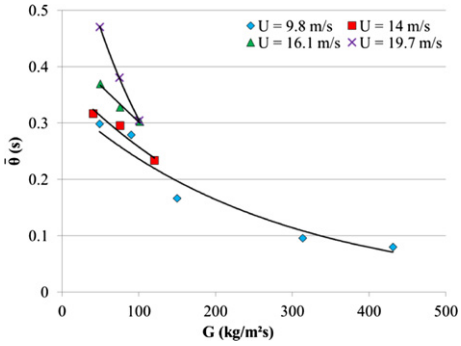

Fig. 10. Fitting contact time $\bar{\theta}$ for different combinations of U and G.

obtained, by using a modified equation for G_{sh} as function of the suspension density ρ_{sus}, being:

$$G_{sh} = 0.014, \text{ for } \rho_{sus} \geq 12 \text{ kg/m}^3 \text{ (hence in the DRU mode)} \tag{17}$$

$$G_{sh} = 0.014 + 0.006\,(12 - \rho_{sus}), \text{ for } \rho_{sus} < 12 \text{ kg/m}^3 \text{ (hence in CAF or DRF mode)} \tag{18}$$

Applying these Equations (17) and (18) into the Gorliz–Grace model, predicts values of the heat transfer coefficient, for all examined flow modes, within ±10% of the experimental value, as illustrated in Fig. 9B.

4.4. Surface removal model

Comparing experimental h_m values with predictions using Equation (11) enables the determination of the required fitting $\bar{\theta}$. This $\bar{\theta}$ value is represented in Fig. 10.

The fitting value of $\bar{\theta}$ and the trend of its dependency on (U,G) again stresses the importance of the riser operating mode. At high values of G, irrespective of U, the riser operates in the DRU (dense upwards flow) mode, and the contact time is determined by the prevailing solids velocity. This velocity is close to the operating gas velocity, according to Equation (2) with $\varepsilon \sim 0.9$ and $\varphi \sim 0.1$ s. In the CAF regime, for $G < \sim 100$ kg/m^{2}s, the contact time is a function of the downward velocity is normally assumed to be close to the terminal velocity of the particles, i.e. 0.38 m/s for the tested particles.

For the heater length of 0.1 m, the contact time should hence be close to 0.26 s, in fair agreement with the experimental fitting results. The application of the contact time approach therefore certainly merits further investigations. These will combine heat transfer measurements and particle residence time measurements by Positron Emission Particle Tracking. Experiments are programmed for September 2012 and will be reported in a follow-up paper.

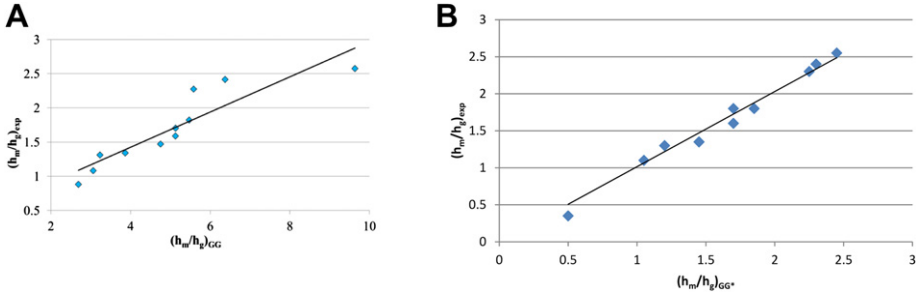

Fig. 9. A. Comparison of experimental and Golriz–Grace (GG) predicted values of h_m/h_g (for $G < \sim 100$ kg/m^{2}s), B. comparison of experimental and Golriz–Grace (GG) predicted values of h_m/h_g (for $G < \sim 100$ kg/m^{2}s) using the modified G_{sh} approach of Equations (17) and (18).

5. Conclusions and recommendations

The present research measured the wall-to-bed heat transfer coefficient in the riser. Measured heat transfer coefficients increase with increasing solid flux at equal values of the gas velocity, and achieve values of ~60 W/m^{2}K at low G and high U values, and up to 350 W/m^{2}K at G ~500 kg/m^{2}s.

The ratio of the suspension heat transfer coefficient and the convective transfer coefficient for the sole gas flow is confirmed as a valid fitting parameter. The application of Molodtsof and Muzyka requires the determination of 2 empirical constants by using the experimental results. Once best fit values of these coefficients are obtained, the correlation predicts the correct trend of the evolution in heat transfer coefficient with U and G.

Within the core–annulus flow regime, the equation of Golriz and Grace, together with the assumptions of its composing parameters, overestimates the experimental results by a factor of about 3. The equations are very sensitive to the values of the estimated parameters, especially G_{sh}. Modified equations for G_{sh} were proposed to fit experimental and predicted results.

When applying a packet renewal mechanism to predict the heat transfer coefficient, the definition of a contact time on the basis of particle velocities in the riser, highly different in function of the riser operating regime, very fairly predicts heat transfer coefficient values. Further research coupling heat transfer measurements and particle contact times (as measured by Positron Emission Particle Tracking) are needed to improve the renewal approach.

Acknowledgements

Authors acknowledge the European Commission for co-funding the “CSP2” Project-Concentrated Solar Power in Particles – (FP7, Project N° 282 932). Further supported was provided by the UK Engineering and Physical Science Research Council (EPSRC grant number: EP/F061439/1), by the Centre for the Innovation in Energy of UAI and FONDECYT No. 1120490 (Chile), and by the National Natural Science Foundation of China (Grants 51176110 and 51071184). The support and advice of Prof. C.Y. Zhao (School of Mechanical Engineering, Shanghai Jiaotong University, Shanghai 200240, China) is highly appreciated.

References

[1] European Union. 7th. framework program for research and technical development CSP2 concentrated solar power in particles, EU grant reference: 282932, 2011.
[2] Mahmoudi S, Chan CW, Brems A, Seville J, Baeyens J. Solids flow diagram of a CFB riser using Geldart B-type powders. Particuology 2012;10:51–61.
[3] Chan CW, Seville JPK, Parker DJ, Baeyens J. Particle velocities and their residence time distribution in the riser of a CFB. Powder Technol 2010;203:187–97.
[4] Fernandes D, Pitié F, Caceres G, Baeyens J. Thermal energy storage: ‘How previous findings determine current research priorities’. Energy 2012;39:246–57.
[5] Baeyens J, Geldart D. Modelling approach the effect of equipment scale on fluidized bed heat transfer data. J Powder Bulk Solids Technol 1980;4:1–9.
[6] Wu RL, Grace JR, Lim CJ, Brereton CMH. Suspension-to-Surface heat transfer in a circulating-fluidized-bed combustor. AIChE J 1989;35:1685–91.
[7] Kunii D, Levenspiel O. [Chapter 11]. Fluidization engineering. Boston (USA): Butterworth-Heinemann; 1991. p. 257–76.
[8] Chen JC, Grace JR, Golriz MR. Heat transfer in fluidized beds: design methods. Powder Technol 2005;150:123–32.
[9] Golriz M, Grace JR. Predicting heat transfer in large-scale CFB boilers. In: Grace JR, Zhu J, de Lasa HI, editors. Circulating fluidized bed technology, vol. VII. Ottawa, ON, Canada: Canadian Society for Chemical Engineering; 2002. p. 121–8.
[10] Mahmoudi S, Baeyens J, Seville J. The solids flow in the CFB-riser quantified by single radioactive particle tracking. Powder Technol 2011;211:135–43.
[11] Chan CW, Seville J, Yang Z, Baeyens J. Particle motion in the CFB riser with special emphasis on PEPT-imaging of the bottom section. Powder Technol 2009;196:318–25.
[12] Hartge EU, Rensner D, Werther J. Solids concentration and velocity patterns in circulating fluidized beds. In: Basu P, Large JF, editors. Circulating fluidized bed technology, vol. II. Oxford, England: Pergamon Press; 1988. p. 165–80.
[13] Matsen JM. Some characteristics of large solids circulation systems. In: Keairns DL, editor. Fluidization technology, vol. 2. New York, N.Y.: Hemisphere Pub. Corp.; 1976. p. 135.
[14] Ouyang S, Potter OE. Consistency of circulating fluidized bed experimental data. Ind Eng Chem Res 1993;32:1041–5.
[15] King DF. Estimation of dense bed voidage in fast and slow fluidized beds of FCC catalyst. In: Grace JR, Shemilt LW, Bergougnou MA, Engineering Foundation (U.S.), editors. Fluidization, vol. VI. New York: Engineering Foundation; 1989. p. 1–8.
[16] Mahmoudi S, Seville JPK, Baeyens J. The residence time distribution and mixing of the gas phase in the riser of a circulating fluidized bed. Powder Technol 2010;203(2):322–30.
[17] Smolders K, Baeyens J. Gas fluidized beds operating at high velocities: a critical review of occurring regimes. Powder Technol 2001;119:269–91.
[18] Smolders K, Baeyens J. Hydrodynamic modelling of the axial density profile in the riser of a low-density circulating fluidized bed. Can J Chem Eng 2001;79:422–9.
[19] Muzyka DW. Use of probabilistic multiphase flow equations in the study of the hydrodynamics and heat transfer in gas-solids suspensions. Ph.D. thesis. University of Western Ontario; 1985.
[20] Grace JR. Heat transfer in high velocity fluidized beds. In: Hetsroni G, editor. Heat transfer 1990, vol. 4. New York: Hemisphere; 1990. p. 329–39.
[21] Basu P, Nag PK. An investigation into heat transfer in circulating fluidized beds. Int J Heat Mass Transf 1987;30:2399–409.
[22] Molodstof Y, Muzyka DW, Large JF, Bergougnou MA. The use of asymptotic similar solutions to probabilistic multiphase flow equations to predict heat transfer rates to dilute gas-solids suspension. Proceedings of the XVIth I.C.N.M.T. symposium. Dubrovnik, Yugoslavia: 1984.
[23] Molodtsof Y, Muzyka DW. General probabilistic multiphase flow equations for analyzing gas-solids mixtures. Int J Eng Fluid Mech 1989;2:1–24.
[24] Molodstof Y. Equations Générales Probabilistes des Écoulements Polyphasiques et Applications aux Mélanges Gaz-Solides. Ph.D. thesis. Université de Technologie de Compiègne; 1985.
[25] Azzi M. Etude des profils de flux de particules dans l'écoulement vertical établi d'une suspension gaz-solide. Ph.D. thesis. Université de Technologie de Compiègne; 1986.
[26] Monceaux L, Azzi M, Molodstof Y, Large JF. Particle mass flux profiles and flow regime characterization in a pilot-scale fast fluidized bed unit. In: Østergaard K, Sorensen A, editors. Fluidization, vol V. New York, N.Y: Engineering Foundation; 1986. p. 337–44.
[27] Tien CL, Quan V. Local heat transfer characteristics of air-glass and air lead mixtures in turbulent pipe flow. ASME; 1962. 62-HT-15: p. 1–9.
[28] Dutta A, Basu P. An improvement of cluster-renewal model for estimation of heat transfer on the water-walls of commercial CFB boilers. 17th international conference on fluidized bed combustion, vol. FBC2003-024. New York: ASME; 2003. p. 235–44.
[29] Welty JR. Engineering heat transfer. New York, N.Y.: John Wiley and Sons; 1974. p. 262.
[30] Lints MCL, Glicksman LR. The structure of particle clusters near the wall of a circulating fluidized bed. In: Weimer AW, editor. Fluid-particle processes, vol. 89. New York, N.Y.: American Institute of Chemical Engineers; 1993. p. 35–52.
[31] Baskakov AP. Heat transfer in fluidised beds: radiative heat transfer, [Chapter 13B]. In: Fluidisation. 2nd ed., Davidson JF, Clift R, Harrison D, editors, London: Academic Press; p. 465–72.
[32] Everaert K, Baeyens J, Smolders K. Heat transfer from a single tube to the flowing gas-solid suspension in a CFB riser. Heat Tran Eng 2006;27:66–70.
[33] Gnielinski V. Fundamentals of heat and mass transfer. Hoboken, N.J.: John Wiley; 2007. p. 514–5.